Phase Behavior of Nanoparticle/Diblock Copolymer Complex in a Selective Solvent

Chieh-Tsung Lo,[†] Byeongdu Lee,[†] Randall E. Winans,[†,‡] and P. Thiyagarajan*[,§]

X-ray Science Division, Chemistry Division, and Intense Pulsed Neutron Source, Argonne National Laboratory, Argonne, Illinois 60439

Received August 23, 2006; Revised Manuscript Received November 15, 2006

ABSTRACT: Solvents used for controlling the self-assembly of polymer nanocomposites have a strong influence on the order−disorder and order−order transition temperatures. We have investigated the phase behavior of complexes composed of poly(styrene-*b*-2-vinylpyridine) (PS−PVP) and thiol-terminated PS stabilized Au nanoparticles in toluene-*d* (a good solvent for PS) by using small-angle neutron scattering. We observe that the morphologies of the neat and nanoparticle-containing polymer solutions strongly depend on the concentration of nanoparticles and temperature. Comparison of the phase diagrams of the neat and nanoparticle-containing polymer solutions as a function of temperature clearly shows dramatic shifts in the order−disorder and order−order transition temperatures. This dramatic effect can be understood by a model wherein the added nanoparticles that sequester in the preferred PS domains increase the interfacial curvature, leading to the observed changes in the nanostructure of the complex. Some effects are similar to those of the selective solvent such as toluene on the nanostructure of PS−PVP. Knowledge gained from these studies on the effects of nanoparticle concentration and temperature on the phase behavior of the polymer nanocomposites will be valuable for tailoring the physical properties of novel nanocomposites.

Introduction

Self-organization of nanoparticles in polymer matrices offers a powerful route to design novel materials as they combine the characteristics of both constituents. Furthermore, the properties of nanocomposites strongly depend on the nature of organization of the nanoparticle building blocks in the matrix. As miniaturization of devices for advanced technologies continues to evolve, advancement in nanotechnology requires novel approaches to engineer composites with nanoparticles well-dispersed as well as organized in defined patterns in a variety of matrices. Recently, it has been suggested that block copolymers exhibiting rich phase behavior at nanoscale can serve as versatile platforms for creating composites with organized nanoparticles in 2D or 3D arrays. Strategies for the fabrication of such copolymer/nanoparticle nanocomposites focus on the direct incorporation of nanoparticles in a selective domain of diblock copolymers by manipulating the specific interactions between nanoparticles with the two segments.[1−11] Subsequent thermodynamically driven microphase separation of block copolymers can then be used to organize the nanoparticles into well-defined patterns in the polymer matrix. These spatially regular nanocomposites could potentially be used in various nanotechnological applications exploiting their magnetic,[12] optical,[13−16] electrical,[17,18] and mechanical properties.[19]

Both theoretical and experimental research have been conducted to understand the effects of nanoparticle size,[8,11,20−24] concentration,[20,21,25−28] shape,[29,30] grafts on nanoparticles,[4−6] and the relative size of blocks of the copolymers[20,23] on the morphology of polymer nanocomposites. It has been observed that the specific distribution of particles in block copolymers depends on the volume fraction of two microdomains and particle concentration, and the morphology of nanocomposites can be tuned to assume any of the ordered phases such as lamellar (L), cylindrical (C), gyroid (G), and spherical (S) structures with particles in the preferred domain. Furthermore, the relative location of particles either in the preferred domain or at the interface can be controlled by varying the particle size and the length and density of the polymer grafts on the particles. However, only recently the subject of solvent effects on the manipulation of the morphology of nanocomposites is being considered.[31]

The addition of a solvent to block copolymers can expand the range of accessible self-assembled morphologies.[32−44] In these studies, solvent selectivity plays an important role on the phase behavior of block copolymers. In a neutral solvent, the solvent equally distributes in both microdomains of the copolymer, leading to lower the order−disorder transition temperature. This behavior is similar to the effect of temperature on the phase behavior of block copolymers. On the other hand, in a selective solvent, the solvent partitions and expands the preferred domain and causes changes in the interfacial curvature. This spontaneous change in interfacial curvature leads to an order−order transition in the morphology of block copolymers. Similarly, the dilution by a selective solvent also can cause the reduction in order−disorder transition temperature. Strong dependence of solvent selectivity on temperature can potentially be exploited for the creation of novel nanocomposites with defined nanoparticle organization.

In this article, we report the phase behavior of the complex of poly(styrene-*b*-2-vinylpyridine) (PS−PVP) block copolymer/Au nanoparticle in toluene, a PS selective solvent. Recently, we demonstrated that the addition of nanoparticles into the PS domain produces significant effects on the phase behavior of the PS−PVP block copolymer.[31] To understand how the solvent and nanoparticles, together, influence the phase behavior of block copolymers, we extended our investigation on the phase behavior of block copolymer/nanoparticle complexes as a function of the concentration of copolymers and the volume fraction of nanoparticles in a selective solvent. This study clearly

* To whom all correspondence should be addressed: thiyaga@anl.gov.
[†] X-ray Science Division, Argonne National Laboratory.
[‡] Chemistry Division, Argonne National Laboratory.
[§] Intense Pulsed Neutron Source, Argonne National Laboratory.

10.1021/ma061950t CCC: $37.00
Published on Web 12/22/2006

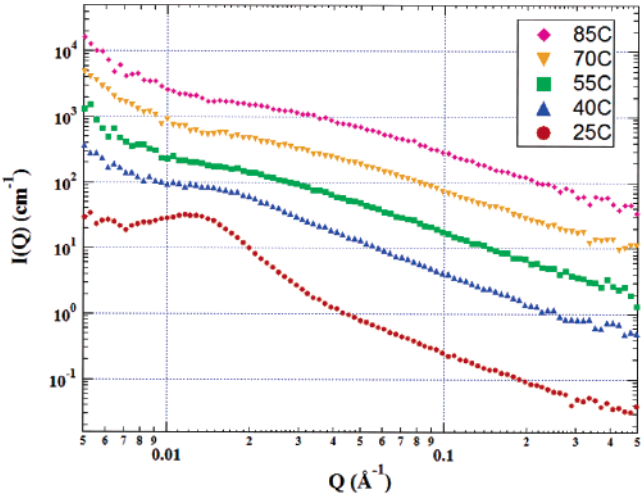

Figure 1. SANS data of neat PS−PVP ($\phi_{PS-PVP} = 8.0\%$) in toluene-*d* as a function of temperature.

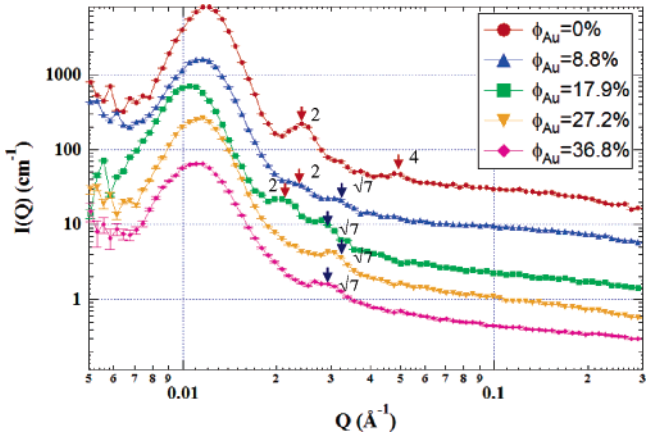

Figure 2. Representative SANS data of neat PS−PVP and its complex with nanoparticles in toluene-*d* ($\phi_{PS-PVP/Au}$ = 43−44%) at 25 °C (scattering patterns have been shifted to increase clarity, and the numbers in the plot show the ratio of the peak positions to the Q^* value of the first-order peak).

shows the effects of nanoparticles in causing dramatic shifts in the order−disorder and order−order transition temperatures of the polymer/nanoparticle complex. This effect can be understood by a model wherein the temperature-dependent difference in the ability of the solvent and the nanoparticles to distribute between the polymer domains of the block copolymer causing interesting changes in the interfacial curvature leading to the observed phase behavior of the complex.

Experimental Section

Au nanoparticles were synthesized by the addition of 1.0 M lithium triethylborohydride (Aldrich Chemical Co., Inc.) to a solution of hydrogen tetrachloroaureate(III) trihydrate (Aldrich Chemical Co., Inc.) and thiol-terminated PS (M_n = 1500 g/mol, PDI = 1.10, Polymer Source, Inc.) in THF (≥99.9%, Aldrich Chemical Co., Inc.).[31,45] The thiol-terminated PS grafts, in addition to providing good protection for nanoparticles from aggregation, enables their confinement in the PS domain of the block copolymer matrix. The purified nanoparticles using methanol (≥99.8%, Aldrich Chemical Co., Inc.) have an average diameter of ~3.6 nm. The Au nanoparticles were then mixed with PS−PVP (M_n = 96 800, f_{PS} = 0.57, PDI = 1.04, Polymer Source, Inc.) in toluene-*d* (99.6% D, Aldrich Chemical Co., Inc.). The solution of PS−PVP/Au complex was stored for at least 3 days prior to the small-angle neutron scattering (SANS) measurements to ensure complete equilibration. As pointed out in our earlier paper,[31] the presence of Au nanoparticles produces strong SAXS signals that mask the scattering signals from the polymer phase and hence we used SANS to investigate the phase behavior of the PS−PVP/Au complexes in toluene-*d*.

SANS experiments were performed using the time-of-flight SAND instrument at the Intense Pulsed Neutron Source in Argonne National Laboratory. A series of solution samples in Suprasil cells with 1 mm path length were loaded in a sample changer that can be maintained at different temperatures. At each temperature the samples were equilibrated for at least 2 h prior to SANS measurements. At this concentration range the phase behavior is thermodynamically driven. Data were collected and reduced in the Q range 0.004−0.3 Å^{-1}, where $Q = (4\pi/\lambda) \sin\theta$, 2θ is the scattering angle, and λ is the wavelength. Corrections for the background from the empty cell, parasitic scattering and absorption were carried out following routine procedures.

Results and Discussion

Figure 1 shows the SANS data for $\phi_{PS-PVP/Au} \sim 8.0\%$ $\phi_{PS-PVP/Au} = (V_{PS-PVP} + V_{Au})/(V_{PS-PVP} + V_{Au} + V_{toluene}) \times 100\%$, assuming additivity of volumes, and V_{PS-PVP}, V_{Au} and $V_{toluene}$ are the volumes of PS−PVP, PS grafted Au nanoparticles, and toluene-*d*, respectively) exhibiting a broad peak, implying the presence of interparticle correlation between micelles formed. The intensity of the peaks decreases with increasing temperature and the peak disappears at higher temperatures, indicating the reduction in the interaction between micelles. The increase in the scattering signal in the low Q region is a signature for their association. At ϕ_{PS-PVP} (volume fraction of neat block polymers in toluene-*d*) and $\phi_{PS-PVP/Au} >$ 15%, ordering in the organization of the micelles starts as indicated by the presence of higher order peaks in the scattering data. Figure 2 shows the representative SANS patterns of neat PS−PVP and its complex with PS grafted Au nanoparticles in toluene-*d* at 25 °C. The volume fraction of the complex in solution is 43−44% and the volume fraction of nanoparticles (ϕ_{Au}) is defined as $\phi_{Au} = V_{Au}/(V_{PS-PVP} + V_{Au}) \times 100\%$. From the SANS data the morphologies, such as lamellar, cylinder, gyroid and disordered, in the PS−PVP/Au complex in toluene-*d* can be characterized by using the Q values of the first-order Q^* and the higher order peaks and the interplanar spacing of the system (d^*) can be calculated using the Q^* value in eq 1.

$$d^* = \frac{2\pi}{Q^*} \tag{1}$$

The morphology and domain spacing of both neat PS−PVP and the complex in toluene-*d* as a function of ϕ_{Au}, $\phi_{PS-PVP/Au}$, and temperature are compiled in Table 1. In Figure 2, at $\phi_{Au} =$ 0%, the strong diffraction peaks correspond to the L phase. It is likely that there may exist a very small fraction of other morphology based on the faint feature in the data. On the basis of the dominant peaks we assign only the L phase for that particular condition. At some conditions (e.g., $\phi_{Au} = 8.8\%$ and 17.9%) coexistence of morphologies has been observed. The assignment of coexisting phases is based on comparable intensities of the peaks in the SANS pattern for different morphologies. Details of the phase behavior of the system and the associated mechanism will be discussed in the following sections.

Peak Intensity. The structure factor, $S(Q)$, of block copolymer in a nonselective solvent is given by[46,47]

$$\frac{1}{S(Q)} = \frac{2\phi}{lN}[F(Q) - 2\chi^* N] \tag{2}$$

Table 1. Morphology and Interplanar Spacing of Neat PS−PVP and PS−PVP/Au Complex in Toluene-*d* from SANS data at Different ϕ_{Au}, $\phi_{PS-PVP/Au}$, and Temperatures

		ϕ_{Au} = 0%		ϕ_{Au} = 8.8%		ϕ_{Au} = 17.9%		ϕ_{Au} = 27.2%		ϕ_{Au} = 36.8%	
temp (°C)	$\phi_{PS-PVP/Au}$ (%)	morphology	d^* (nm)	morphology	d^* (nm)	morphology	d^* (nm)	morphology	d^* (nm)	morphology	d^* (nm)
25	16−17	C	50.4	C	45.0	C	46.3	C	47.6	D	
40		C	47.6	D		D		D		D	
55		C	46.3	D		D		D		D	
70		D		D		D		D		D	
85		D		D		D		D		D	
100				D		D		D		D	
25	25−26	C	51.9	C	50.4	C	49.0	C	50.4	C	51.9
40		C	49.0	C	49.0	C	47.6	C	49.0	C	50.4
55		C	47.6	C	47.6	D		D		D	
70		C	47.6	C	47.6	D		D		D	
85		C	47.6	C	46.3	D		D		D	
100				D		D		D		D	
25	34−35	C	53.4	C	51.9	C	54.9	C	51.9	C	54.9
40		C	51.9	C	50.4	C	54.9	C	50.4	C	54.9
55		C	50.4	C	49.0	C	53.4	G + C	49.0	C	53.4
70		L	49.7	C	49.0	C	53.4	G + C	47.6	G	51.9
85		L	49.0	L	47.6	L + C	51.9	G + C	47.6	G	50.4
100		L	47.6	D		L	50.4	G + C	46.3	G	49.0
25	43−44	L	51.9	L + C	53.4	L + C	59.8	C	54.9	C	56.5
40		L	50.4	L	51.9	L + C	58.1	C	53.4	C	54.9
55		L	49.0	L	50.4	L + C	56.5	C	53.4	C	54.9
70		L	47.6	L	50.4	L + C	54.9	C	51.9	G	53.4
85		L	47.6	L	49.0	L	53.4	C	50.4	G	51.9
100				L	47.6	L	51.9	G + C	50.4	D	

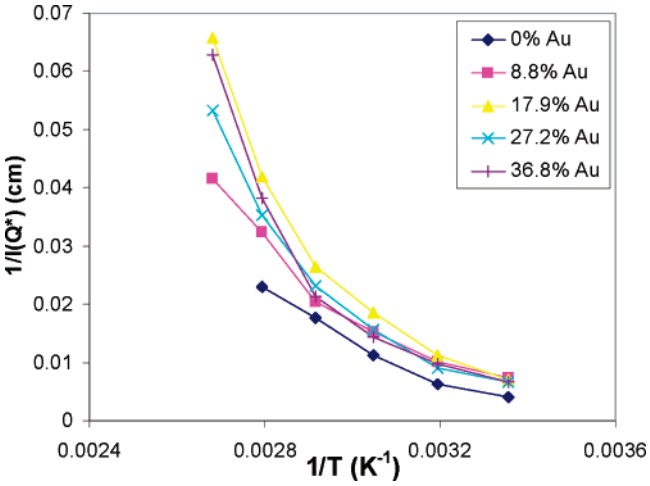

Figure 3. SANS peak intensity at $Q = Q^*$ as a function of temperature for neat PS−PVP and its complex with nanoparticles in toluene-*d* ($\phi_{PS-PVP/Au}$ = 24−25%).

Here ϕ is the volume fraction of polymer solution, *l*, the segment length of the block copolymer and N, the degree of polymerization. $F(Q)$ is related to the radius of gyration and composition of the block copolymer, and χ^* is the effective interaction parameter between the monomers. In a selective solvent, the effective segregation described by χ^*N, can be modified as[48]

$$\chi^*N = \phi(\chi + \delta\chi_s)N \tag{3}$$

Here $\delta\chi_s$ is the difference in interaction parameter between the selective solvent and the two monomers. The value is assumed to be 0 for a neutral solvent and 0.05 for poly(styrene-*b*-isoprene) in di-*n*-butyl phthalate that is a good solvent for isoprene.[37] χ is the interaction parameter of two monomers of the blocks, that is inversely proportional to the temperature. Equation 2 implies that $I(Q^*)^{-1}$, is proportional to T^{-1} in a neutral solvent, where *T* is the temperature. Figure 3 shows the SANS peak intensity at $Q = Q^*$ as a function of inverse temperature for neat PS−PVP and the complex ($\phi_{PS-PVP/Au}$ = 24−25%) in toluene-*d*. It is clearly seen that while the curve is slightly nonlinear with temperature for the neat block copolymer solution, its nonlinearity monotonically increases with increasing nanoparticle concentration and temperature, indicating the enhanced compositional fluctuations in the solution of the complex.[49] These fluctuations are significant at higher temperatures because the solvent becomes more neutral to the system, due to the upper critical solution temperature behavior of PS and PVP,[50] and it redistributes to the PVP domain. Similarly, at these temperatures, the interaction energy between the PS grafted nanoparticles and PVP domains also reduces that increases the potential for its redistribution. However, their diffusion will be very low when compared to the solvent due to entanglement between chains in the grafts and matrix and the additional entropic penlalty.[31] These fluctuation effects significantly influence the equilibrium properties of the microphase separation behavior of the complex in solution.

Domain Spacing. Since the nanoparticles and the solvent can swell the PS domain, it would be interesting to analyze the domain spacing as a function of both nanoparticle concentration and the volume fraction of the PS−PVP/Au complex. In neutral solvents, both experimental[32,51,52] and theoretical predictions[46,53] revealed the following relationship between d^* and ϕ at high polymer volume fraction:

$$d^* \sim \phi^{1/3} \tag{4}$$

In selective solvents, d^* strongly depends on the solvent selectivity. In a highly selective solvent, d^* increases in the lamellar phase due to chain stretching to reduce their interfacial area with the added solvents.[38] Self-consistent theory[54] reveals that the exponent in the lamellar phase in a neutral solvent vary from 0.4 in the strong segregation regime to 0.2 in the weak segregation regime. As the selectivity decreases with increasing temperature, the scaling law approaches that of the neutral solvent as shown in eq 4. Banaszak and Whitmore[54] also described the scaling law of block copolymers in a selective solvent using self-consistent theory. They reported that the exponents change from 0.2 in the weak segregation regime to

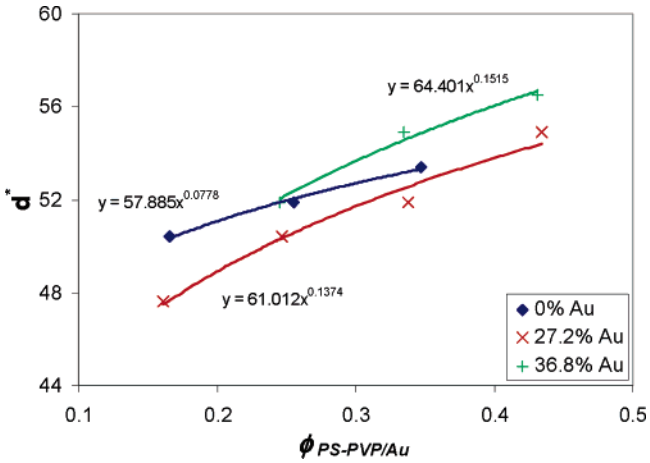

Figure 4. Domain size d^* for the cylinder phase at 25 °C as a function of polymer concentration ($\phi_{PS-PVP/Au}$) at different particle loading. The lines are fits using an exponential function.

0.03 in the strong segregation regime, and these values significantly differ from those for a neutral solvent. This decreasing segregation in a selective solvent allows the chains to increase their stretching normal to the interface. To quantify d^* in a selective solvent, Lai et al.[39] modified eq 4 using the dimensionality of the lattice (n) and the microdomain interfacial area per chain (A_c)

$$d^* \sim A_c^{-1}\phi^{-1/n} \tag{5}$$

where $n = 1$ for lamellae, 2 for cylinders and 3 for spheres of the insoluble block. Assuming that A_c is proportional to ϕ^{-a}, eq 5 can be written as

$$d^* \sim \phi^{a-1/n} \tag{6}$$

Here, a is a function of both the solvent selectivity and morphology, and its value decreases in the order L > C > S. Consequently, the exponent ($a - 1/n$) increases with decreasing solvent selectivity and degree of segregation in a selective solvent. Below we discuss the behavior of domain spacing in different polymer phases of the PS−PVP/Au complex in light of the above formalism.

Because of the very few L phases observed in our SANS experiments we could not derive a scaling law for this phase. However, we observe that for neat PS−PVP in a selective solvent, d^* decreases with increasing ϕ_{PS-PVP}. Table 1 shows that, at 70 °C, $d^* = 49.7$ nm in 34.7% and 47.6 nm at 44.4% ϕ_{PS-PVP} and, at 85 °C, $d^* = 49.0$ nm in 34.7% and 47.6 nm in 44.4% ϕ_{PS-PVP}, indicating an exponent that is negative for the neat polymer solution. With the addition of nanoparticles, a significant difference in the exponent is observed. At $\phi_{Au} = 8.8\%$, d^* increases from 47.6 to 49.0 nm as $\phi_{PS-PVP/Au}$ increases from 34.4% to 44.0% at 85 °C. A similar behavior was observed for $\phi_{Au} = 17.9\%$ in $\phi_{PS-PVP/Au} = 34.1\%$ and 43.7% at 100 °C. Thus, the addition of nanoparticles increases the value of the exponent. Such a behavior is also seen for the C phase. Figure 4 illustrates the effect of particle loading on d^* for cylindrical morphology as a function of PS−PVP/Au concentration at 25 °C. Although the observed SANS peaks are broad due to the relatively moderate resolution and the small coherence lengths of the domains, we still can observe definite trends on the effect of nanoparticles on d^* in PS−PVP in toluene. In the case of neat block copolymer solutions the exponent that is negative for the L phase becomes slightly positive (0.078) for the C phase and this is consistent with the experimental results

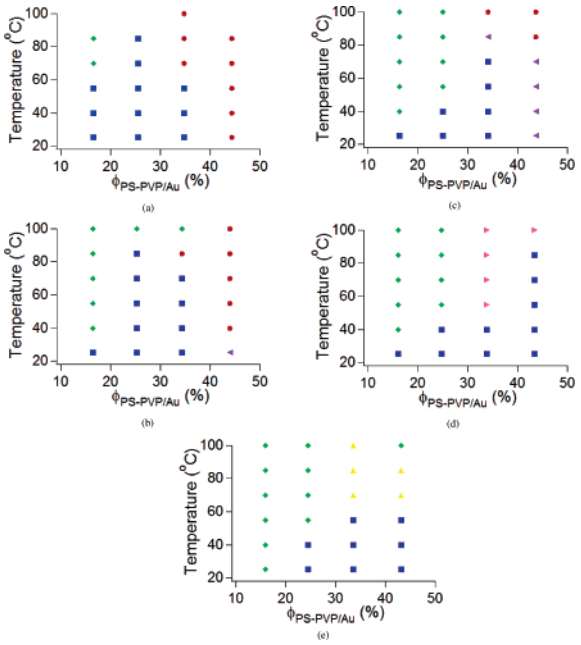

Figure 5. Phase diagram of PS−PVP/Au in toluene-d as a function of temperature and polymer concentration: (a) neat block copolymer; (b) $\phi_{Au} = 8.8\%$; (c) $\phi_{Au} = 17.9\%$; (d) $\phi_{Au} = 27.2\%$; and (e) $\phi_{Au} = 36.8\%$. Key: (●) L; (solid triangle pointing left) L + C; (▲) G; (solid triangle pointing right) G + C; (■) C; (◆) D.

of poly(styrene-*b*-isoprene) in a isoprene-selective solvent.[39] It can be seen from Figure 4 that the value of the exponent for the C phase increases from 0.137 to 0.152 when ϕ_{Au} increases from 27.2% to 36.8%. This behavior can be attributed to the reduced segregation of microdomains in the presence of nanoparticles,[20] as predicted by the self-consistent theory.[54]

Phase Behavior. The phase diagrams based on the SANS data of neat and PS−PVP/Au complexes at different Au concentration in toluene-d are presented in Figure 5. Figure 5a shows the morphology of neat PS−PVP in toluene-d as functions of temperature and ϕ_{PS-PVP}. Contrary to the lamellar morphology expected for the PS−PVP melt, the solution sample with $\phi_{PS-PVP} = 16.6\%$ exhibits a cylindrical structure at low temperature. Swelling of the PS domain by the selective solvent is the cause for this morphological transformation. At $T >$ 70 °C, an order−disorder transition occurs. Furthermore, the presence of solvent increases the degree of freedom for the system to lower its free energy. At very low ϕ_{PS-PVP} the system can undergo a macrophase separation into the solvent-rich disordered phase.[35] At $\phi_{PS-PVP} = 25.5\%$, it exhibits a cylindrical structure in the entire temperature range considered here. At this concentration, the density of the chain entanglements with neighbors will become higher and this increases the order−disorder transition temperature. At $\phi_{PS-PVP} = 34.7\%$, the swelling of the PS domain by the solvent decreases with increasing temperature, due to its decreasing selectivity and redistribution in PS to PVP domains. At $T >$ 70 °C, the amount of toluene-d required to make a phase transition to cylindrical phase is insufficient, and thus the system remains in the lamellar morphology expected in the bulk. At still higher polymer concentration ($\phi_{PS-PVP} = 44.4\%$), neat PS−PVP in toluene-d exhibits a lamellar structure in a wide temperature range of 25 to 100 °C. The schematic of the mechanism by which the phase transitions occur for the PS−PVP in toluene-d with increasing temperature is illustrated in Figure 6a.

Addition of a PS-grafted Au nanoparticle has a significant influence on the phase behavior of PS−PVP. In the sample with

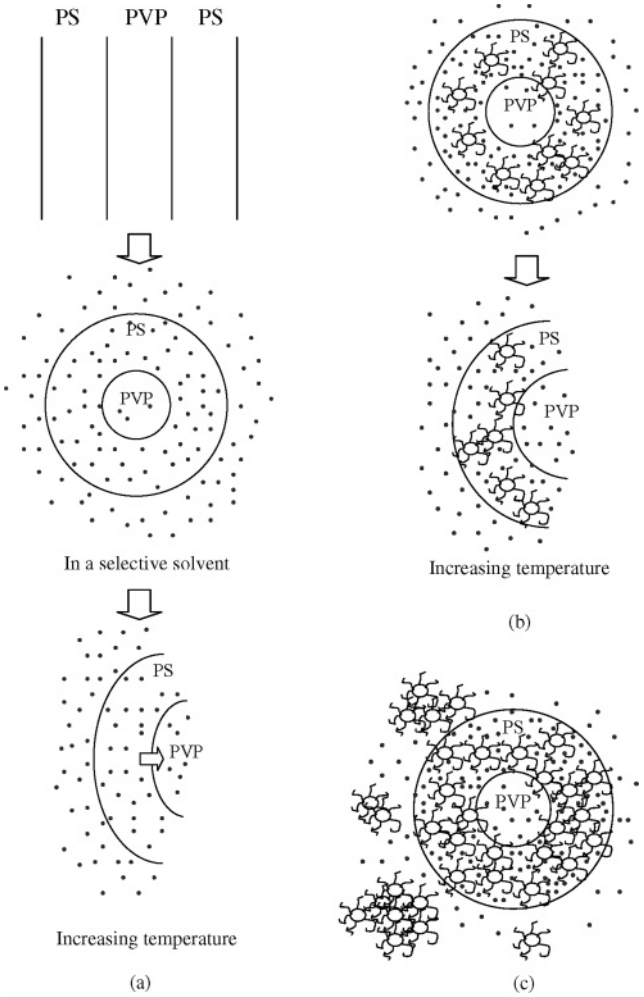

Figure 6. Schematics of the mechanism of phase transitions in (a) neat PS−PVP in toluene-*d*, (b) PS−PVP/Au in toluene-*d*, and (c) PS−PVP/Au with high particle loading in toluene-*d*. (Small circles and big circles with chains indicate solvent and thiol-terminated grafted Au nanoparticles, respectively.)

$\phi_{PS-PVP/Au} = 16.4\%$ and $\phi_{Au} = 8.8\%$ (Figure 5(b)), the order−disorder transition (ODT) temperature decreases from about 70 to 40 °C. Interestingly, for both $\phi_{PS-PVP/Au} = 25.2\%$ and 34.4% at similar nanoparticle concentrations, the ODT remains at 100 °C. This indicates that the presence of nanoparticles at sufficient concentration can significantly weaken the degree of segregation and cause a vertical shift in the phase map. At a much higher nanoparticle loading, a macrophase separation of nanoparticles occurs, resulting in a decrease in ODT.[20] This effect of nanoparticles is quite different from that caused by the homopolymers that can selectively sequester in the preferred domain, as unlike the nanoparticles, they do not modify the degree of segregation but only affect the volume expansion of the target domain, causing a horizontal shift in the phase diagram.[55] At $\phi_{PS-PVP/Au} = 34.4\%$, the order−order transition temperature (OOT) increases from 70 °C in neat PS−PVP to 85 °C in PS−PVP/Au. This can be attributed to the swelling of PS domain by the nanoparticles, which is reminiscent of the behavior of the selective solvents. However, while the solvent can distribute to the PVP domain at higher temperatures as depicted in Figure 6b, the diffusion of the nanoparticles is much slower due to the entanglements between the chains in the grafts and the matrix as well as the additional entropic penalty. This difference in their ability to distribute between the polymer domains limits the changes in the overall interfacial curvature, causing slow transitions in the block copolymer phase behavior.

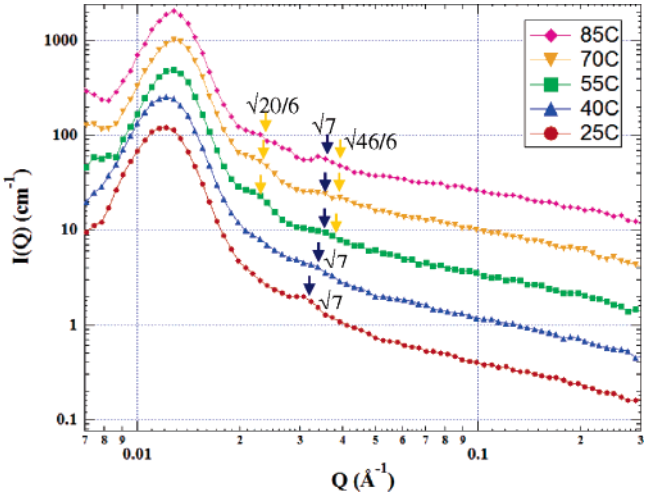

Figure 7. SANS data of neat PS−PVP ($\phi_{PS-PVP} = 33.8\%$) and its complex with Au ($\phi_{Au} = 27.2\%$) in toluene-*d* as a function of temperature (scattering patterns have been shifted to increase clarity, and the numbers in the plot show the ratio of the peak positions to the Q^* value of the first-order peak).

At $\phi_{PS-PVP/Au} = 44.0\%$ and $\phi_{Au} = 8.8\%$ and 17.9%, lamellar and cylindrical phases coexist at 25 °C (Figure 2), which may be due to the heterogeneous distribution of the nanoparticles and solvent in the polymer phase, modifying the interfacial curvatures to different extents. The coexisting phases cause packing frustration leading to transitions from gyroid to lamellar and cylindrical structures.[41]

For samples with $\phi_{PS-PVP/Au} = 34.1\%$ and $\phi_{Au} = 17.9\%$ (Figure 5c), additional order−order transitions occur from cylindrical to coexisting lamellar and cylindrical phases at 85 °C as well as coexisting lamellar and cylindrical phases to lamellar at 100 °C. The additional order−order transitions in the presence of nanoparticles enlarge the range of ordered microdomains in the PS−PVP system. A similar behavior was predicted for the block copolymer in a selective solvent by a self-consistent mean-field theory.[35] It was seen that with the increasing solvent selectivity, multiple order−order transitions occur, enriching the phase diagrams. Such increasing ordered and coexisting lamellar and cylindrical phases are also observed for samples with $\phi_{PS-PVP/Au} = 43.7\%$ in the temperature range 25−70 °C.

Figure 5d shows the PS−PVP/Au in toluene-*d* at $\phi_{Au} = 27.2\%$. At higher loading of nanoparticles in PS domains, the interfacial curvature increases significantly and the system becomes more asymmetric. The phase behavior of PS−PVP/Au at low polymer concentration resembles that observed for the sample with $\phi_{Au} = 17.9\%$. However, up to $\phi_{PS-PVP/Au} = 33.8\%$, new coexisting gyroid and cylinder phases are observed at higher temperatures as shown in Figure 7 (broad higher order peak at 85 °C is due to the overlap of peaks corresponding to $Q/Q^* = \sqrt{7}$ and $\sqrt{46}/6$).

The phase behavior of PS−PVP/Au complex in toluene-*d* at $\phi_{Au} = 36.8\%$ is shown in Figure 5e. For this sample an order to disorder transition occurs at lower polymer concentration in a wide temperature range. At this high loading of nanoparticles a macrophase separation of nanoparticles and copolymers can occur as depicted in Figure 6c. However, at higher polymer concentrations ($\phi_{PS-PVP/Au} > 34\%$) and higher particle loading, we observe the cylindrical and gyroid structures. As expected, the peak width also becomes larger especially for higher order peaks, indicating the lesser order in the system. It has been reported that the gyroid phase is stable only in weakly segregated

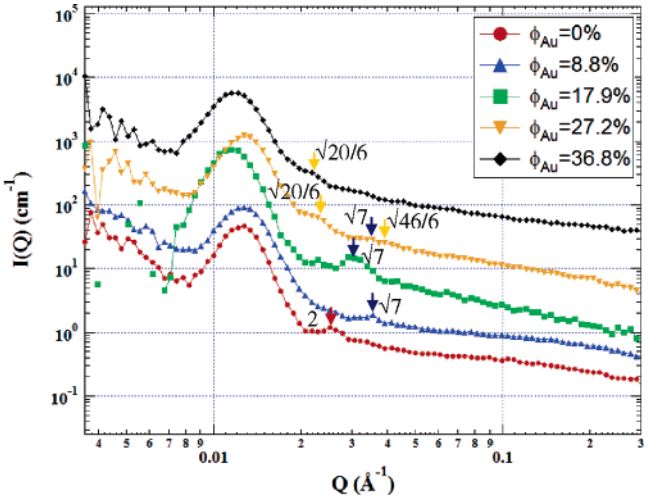

Figure 8. SANS data of neat PS−PVP ($\phi_{PS-PVP/Au}$ = 34%) and its complex with nanoparticles in toluene-*d* at 70 °C (scattering patterns have been shifted to increase clarity, and the numbers in the plot show the ratio of the peak positions to the *Q** value of the first-order peak).

block copolymers.[38] In this study we observe the gyroid phase at high nanoparticle loading and at high temperatures that is quite reasonable based on the weak segregation expected at these conditions.

The sequence of phase transitions exhibited by the bulk PS−PVP from lamellar → gyroid → cylindrical → spherical structures is significantly different for the PS−PVP/Au complex solution. For instance, ∼34% PS−PVP/Au in toluene-*d* at 70 °C exhibits lamellar → cylindrical → cylindrical + gyroid → gyroid as shown by the SANS data in Figure 8. Even though toluene-*d* is selective to PS domain, it still can accumulate at the interface[56] and the PVP domain[54] due to the additional entropic penalty. In PS−PVP/Au complex solution both nanoparticles and solvent compete for the space in the preferred PS domain. To maintain a lower free energy, solvent with higher interaction energy with PS ($\chi_{PS-toluene} \sim 0.4$)[57] will be driven to the PVP domain. In addition, the packing constraints caused by the nanoparticles will exclude the excess solvent to the interface and the PVP domain. These two effects reduce the overall changes in the interfacial curvature and induce the interesting phase transition from cylinder to gyroid.

Conclusion

We investigated the phase behavior of neat and PS−PVP complex with PS grafted Au particles in toluene-*d* using SANS. The morphology of complex in the solvent strongly depends on the particle loading, volume fraction of PS−PVP/Au in the solvent and temperature. The structural changes for this complex can be understood by the spontaneous response of the interfacial curvature due to the swelling of the preferred domain by the solvent and added nanoparticles. At lower temperatures, the solvent and nanoparticles sequester into the selective PS domain and increase the interfacial curvature between the PS and PVP microphase-separated domains. This induces order−order transitions. Their presence enlarges and modifies the PS domain that increases the range of ordered microdomains in the system. At higher particle concentration the packing of nanoparticles in the PS domain reaches a saturation level and this causes the macrophase separation, leading to an order−disorder transition.

As temperature increases the repulsive interaction between PS and PVP reduces and the weakened interfacial tension provides as a driving force for the redistribution of both the solvent and the PS grafted nanoparticles to the PVP domain. While the solvent can readily diffuse, the entanglements and the additional entropic penalty will constrain the diffusion of the nanoparticles. This dramatic difference in their ability to redistribute in the polymer domains limits the changes in the overall interfacial curvature, causing the interesting slow transitions in the block copolymer phase behavior.

Acknowledgment. This work benefited from the use of APS and IPNS funded by DOE-BES under Contract No. DE-AC02-06CH11357. We also appreciate D. G. Wozniak for his assistance in SANS experiments.

References and Notes

(1) Chan, Y. N. C.; Schrock, R. R.; Cohen, R. E. *Chem. Mater.* **1992**, *32*, 24−27.
(2) Chan, Y. N. C.; Craig, G. S. W.; Schrock, R. R.; Cohen, R. E. *Chem. Mater.* **1992**, *4*, 885−894.
(3) Sohn, B. H.; Cohen, R. E. *Acta Polym.* **1996**, *47*, 340−343.
(4) Tsutsumi, K.; Funaki, Y.; Hirokawa, Y.; Hashimoto, T. *Langmuir* **1999**, *15*, 5200−5203.
(5) Hashimoto, T.; Harada, M.; Sakamoto, N. *Macromolecules* **1999**, *32*, 6867−6870.
(6) Okumura, A.; Tsutsumi, K.; Hashimoto, T. *Polym. J.* **2000**, *32*, 520−523.
(7) Sohn, B. H; Seo, B. H. *Chem. Mater.* **2001**, *13*, 1752−1757.
(8) Bockstaller, M. R.; Lapetnikov, Y.; Margel, S.; Thomas, E. L. *J. Am. Chem. Soc.* **2003**, *125*, 5276−5277.
(9) Sohn, B.-H.; Choi, J. -M.; Yoo, S. I.; Yun, S. -H.; Zin, W. -C.; Jung, J. C.; Kanehara, M.; Hirata, T.; Teranishi, T. *J. Am. Chem. Soc.* **2003**, *125*, 6368−6369.
(10) Lin, Y.; Boker, A.; He, J.; Sill, K.; Xiang, H.; Abetz, C.; Li, X.; Wang, J.; Emrick, T.; Long, S.; Wang, Q.; Balazs, A. *Nature (London)* **2005**, *434* (3), 55−59.
(11) Chiu, J. J.; Kim, B. J.; Kramer, E. J.; Pine, D. J. *J. Am. Chem. Soc.* **2005**, *127*, 5036−5037.
(12) Sohn, B. H.; Cohen, R. E. *Chem. Mater.* **1997**, *9*, 264−269.
(13) Maldovan, M.; Urbas, A. M.; Yufa, N.; Carter, W. C.; Thomas, E. L. *Phys. Rev. B* **2002**, *65*, 165123.
(14) Bockstaller, M. R.; Thomas, E. L. *J. Phys. Chem. B* **2003**, *107*, 10017−10024.
(15) Buxton, G. A.; Lee, J. Y.; Balazs, A. C. *Macromolecules* **2003**, *36*, 9631−9637.
(16) Bockstaller, M. R.; Thomas, E. L. *Phys. Rev. Lett.* **2004**, *93*, 166106.
(17) Ciebien, J. F.; Clay, R. T.; Sohn, B. -H.; Cohen, R. E. *New J. Chem.* **1998**, 685−691.
(18) Torquato, S.; Hyun, S.; Donev, A. *Phys. Rev. Lett.* **2002**, *89*, 266601.
(19) Buxton, G. A.; Balazs, A. C. *Phys. Rev. E.* **2003**, *67*, 031802.
(20) Huh, J.; Ginzburg, V. V.; Balazs, A. C. *Macromolecules* **2000**, *33*, 8085−8096.
(21) Thompson, R. B.; Ginzburg, V. V.; Matsen, M. W.; Balazs, A. C. *Science* **2001**, *292*, 2469−2472.
(22) Lee, J.-Y.; Thompson, R. B.; Jasnow, D.; Balazs, A. C. *Phys. Rev. Lett.* **2002**, *89*, 155503.
(23) Lee, J. Y.; Thompson, R. B.; Jasnow, D.; Balazs, A. C. *Macromolecules* **2002**, *35*, 4855−4858.
(24) Lee, J. Y.; Thompson, R. B.; Jasnow, D.; Balazs, A. C. *Faraday Discuss* **2003**, *123*, 121−131.
(25) Yeh, S.-W.; Wei, K.-H.; Sun, Y.-S.; Jeng, U.-S.; Liang, K. S. *Macromolecules* **2003**, *36*, 7903−7907.
(26) Ho, R.-M.; Lin T. Jhong, M.-R.; Chung, T.-M.; Ko, B.-T.; Chen, Y.-C. Macromolecules **2005**, *38*, 8607−8610.
(27) Yeh, S.-W.; Wu, T.-L.; Wei, K.-H.; Sun, Y.-S.; Liang, K. S. *J. Polym. Sci., Polym. Phys. Ed.* **2005**, *43*, 1220−1229.
(28) Yeh, S.-W.; Wei, K.-H.; Sun, Y. S.; Jeng, U.-S.; Liang, K. S. *Macromolecules* **2005**, *38*, 6559−6565.
(29) Jain, A.; Gutmann, J. S.; Garcia, C. B. W.; Zhang, Y.; Tate, M. W.; Gruner, S. M.; Wiesner, U. *Macromolecules* **2002**, *35*, 4862−4865.
(30) Chervanyov, A. I.; Balazs, A. C. *J. Chem. Phys.* **2003**, *119*, 3529−3534.
(31) Lo, C.-T.; Lee, B.; Winans, R. E.; Thiyagarajan, P. *Macromolecules* **2006**, *39*, 6318−6320.
(32) Shibayama, M.; Hashimoto, T.; Hasegawa, H.; Kawai, H. *Macromolecules* **1983**, *16*, 1427−1433.
(33) Shibayama, M.; Hashimoto, T.; Kawai, H. *Macromolecules* **1983**, *16*, 16−28.
(34) Lodge, T. P., Xu, X.; Ryu, C. Y.; Hamley, I. W.; Fairclough, J. P. A.; Ryan, A. J.; Pedersen, J. S. *Macromolecules* **1996**, *29*, 5955−5964.
(35) Huang, C.-I.; Lodge, T. P. *Macromolecules* **1998**, *31*, 3556−3565.

(36) Hamley, I. W.; Fairclough, J. P. A.; Ryan, A. J.; Ryu, C. Y.; Lodge, T. P.; Gleeson, A. J.; Pedersen. J. S. *Macromolecules* **1998**, *31*, 1188−1196.
(37) Hanley, K. J; Lodge, T. P. *J. Polym. Sci., Polym. Phys. Ed.* **1998**, *36*, 3101−3113.
(38) Hanley, K. J.; Lodge, T. P.; Huang, C.-I. *Macromolecules* **2000**, *33*, 5918−5931.
(39) Lai, C.; Russel, W. B.; Register, R. A. *Macromolecules* **2002**, *35*, 4044−4049.
(40) Lai, C.; Russel, W. B.; Register, R. A. *Macromolecules* **2002**, *35*, 841−849.
(41) Lodge, T. P.; Pudil, B.; Hanley, K. J. *Macromolecules* **2002**, *35*, 4707−4717.
(42) Lodge, T. P.; Hanley, K. J.; Pudil, B.; Alahapperuma, V. *Macromolecules* **2003**, *36*, 816−822.
(43) Park, M. J.; Bang, J.; Harada, T.; Char, K.; Lodge, T. P. *Macromolecules* **2004**, *37*, 9064−9075.
(44) Park, M. J.; Char, K.; Bang, J.; Lodge, T. P. *Macromolecules* **2005**, *38*, 2449−2459.
(45) Yee, C. K.; Jordan, R.; Ulman, A.; White, H.; King, A.; Rafailovich, M.; Sokolov, J. *Langmuir* **1999**, *15*, 3486−3491.
(46) Olvera de la Cruz, M. *J. Chem. Phys.* **1989**, *90*, 1995−2002.
(47) Fredrickson, G. H; Leibler, L. *Macromolecules* **1989**, *22*, 1238−1250.
(48) Helfand, E.; Tagami, Y. *J. Chem. Phys.* **1972**, *56*, 3592−3601.
(49) Fredrickson, G. H.; Helfand, E. *J. Chem. Phys.* **1987**, *87*, 697−705.
(50) Schulz, M. F.; Khandpur, A. K.; Bates, F. S.; Almdal, K.; Mortensen, K.; Hajduk, D. A.; Gruner, S. M. *Macromolecules* **1996**, *29*, 2857−2867.
(51) Hashimoto, T.; Shibayama, M.; Kawai, H. *Macromolecules* **1983**, *16*, 1093−1101.
(52) Shibayama, M.; Hashimoto, T.; Kawai, H. *Macromolecules* **1983**, *16*, 1434−1443.
(53) Whitmore, M. D.; Noolandi, J. *J. Chem. Phys.* **1990**, *93*, 2946−2955.
(54) Banaszak, M.; Whitmore, M. D. *Macromolecules* **1992**, *25*, 3406−3412.
(55) Winey, K. I.; Thomas, E. L.; Fetters, L. J. *Macromolecules* **1992**, *25*, 2645−2650.
(56) Lodge, T. P.; Hamersky, M. W.; Hanley, K. J.; Huang, C.-I. *Macromolecules* **1997**, *30*, 6139−6149.
(57) Barton, A. F. M. In *CRC Handbook of Polymer-Liquid Interaction Parameters and Solubility Parameters*; CRC Press, Inc.: Boca Raton, FL, 1990.

MA061950T